

CHAPTER XII

High-resolution IR spectroscopy of jet-cooled allyl radical ($\text{CH}_2\text{-CH-CH}_2$): in-phase (ν_1) and out-of-phase (ν_{13}) antisymmetric CH_2 stretching vibrations

12.1 Introduction

As already discussed in the previous chapter, free radicals play an important role in an impressive variety of environments, ranging from diamond film deposition¹ to combustion chemistry² to molecular synthesis in the interstellar medium.³ Indeed, it is well appreciated that the majority of chemical processes take place via elementary reaction steps involving such highly reactive transient radical species. By virtue of their extreme reactivity, however, detailed study of their kinetic and spectroscopic properties presents an ongoing experimental challenge, often requiring much more sensitive and sophisticated detection methods than those suitable for stable closed shell molecules. Of particular importance in this regard have been high-resolution spectroscopic methods, which in principle offer the exquisite ability to monitor multiple radical species as a function of time in a complex gaseous mixture,^{4,5,6,7} such as routinely encountered in pollution,⁸ combustion,^{9,10,11} or semiconductor plasma etching phenomena.^{1,12,13} This combination of time and frequency domain capabilities permits detailed flash kinetic spectroscopy studies of radicals to be pursued, as first beautifully demonstrated by Pimentel and co-workers.^{14,15} These techniques

have also been later developed to an even more sensitive and elegant level with high-resolution diode, tunable difference frequency, and frequency doubled cw laser sources in the groups of Curl,¹⁶ Moore,¹⁷ Sears,¹⁸ Tully,¹⁹ and others.^{11,13,20,21,22}

Despite the power of these flash kinetic methods, there are limiting sensitivity issues that grow dramatically as a function of radical size for near room temperature conditions. Specifically, these issues arise primarily from a combination of i) dilution of species per quantum state and ii) rovibrational spectral congestion, both due to the rapid increase in partition function with temperature. Both of these experimental problems can be greatly reduced by producing the radicals in a supersonically-cooled expansion, where the population of the molecules is effectively concentrated down into the lowest rotational levels. Indeed, one of the first high-resolution laser spectroscopic studies of jet-cooled radicals was the work of Smalley *et al.* in 1974, which obtained the laser induced fluorescence (LIF) study of the NO₂ molecule in a supersonic free jet.^{23,24}

Over the past two decades, the study of unstable species in jets has been greatly expanded by using photolysis, laser ablation,²⁵ pyrolysis,²⁶ and electric discharges²⁷ for free radical production. The predominant fraction of these studies has been conducted in the visible and UV regions using LIF and multiphoton ionization, with over 75 radical species already spectroscopically characterized²⁸ as of 1995. By way of contrast, there have been comparatively fewer studies of radicals conducted in the infrared and longer spectral regions. Though capabilities for spectroscopic studies of jet-cooled transient species in these regions have been

reported by several groups,^{16,29,30,31,32,33,34,35} high-resolution IR spectroscopy of larger jet-cooled free radicals remains a substantially challenging albeit extremely interesting area of research effort.

Recently, we reported the development of pulsed supersonic slit jet discharges as an unusually intense source of rotationally cold radicals.³⁶ The discharge is generated in a 1 mm long chamber prior to the expansion orifice, which effectively limits secondary chemical reactions to $< 2 \mu\text{s}$ at typical discharge flow velocities before supersonic cooling. This discharge source has been demonstrated to generate radicals in impressive concentrations, which in favorable systems can be as high as $10^{14} - 10^{15}$ radicals/cm³ at the slit expansion orifice. In conjunction with multipass optics and shot noise limited detection sensitivities in the spectrometer, this proves readily sufficient for direct absorption IR studies of jet-cooled transient species at high S/N. As a further bonus, the sub-Doppler resolution that accompanies jet cooling in the slit jet geometry can allow fine and sometimes even hyperfine structure to be fully or partially resolved. In the case of the methyl radical (discussed in the previous chapter), for example, this capability has allowed hyperfine structure and spin-polarization effects to be observed and analyzed for the first time under isolated gas phase conditions.³⁷

In contrast to their ubiquitous importance in chemistry, remarkably few hydrocarbon radicals have been successfully characterized by high-resolution spectroscopy. Hydrocarbon free radicals play a particularly relevant role in the high temperature chemistry of conversion and transformation processes of raw fuel stock, where the combustion processes such as cracking, oxygenation, and

cyclization proceed predominantly through free radicals.² Several small hydrocarbon radicals such as CH, CH₂, and CH₃ have been investigated by both electronic and high-resolution IR spectroscopy.^{18, 28, 37, 42, 43} Longer chain species have been observed by Thaddeus and co-workers^{34, 35} in pulsed jets using a Fourier Transform microwave spectrometer. Very recently, Endo and co-workers³⁸ have observed LIF spectra of C₄H and C₄D in a pulsed discharge nozzle. Flash kinetic spectroscopy has been used with color center lasers by Curl and co-workers for high-resolution studies of C₂H³⁹ and propargyl radicals.⁴⁰ Of special importance to the present work, there have also been flash kinetic spectroscopic studies by Hirota and co-workers of hydrocarbon species such as allyl radical,⁴¹ probed in the CH bend region with tunable diode lasers. Diode lasers have also been used with flash kinetic spectroscopy by Sears and co-workers for extensive investigation of methyl⁴² and ethyl⁴³ radicals. However, even for as deceptively “simple” a radical species as ethyl radical, the degree of spectral complexity under room temperature conditions generates major challenges to detailed rotational assignment, which can be greatly accelerated by spectra obtained under slit jet-cooled discharge conditions.⁴⁴ This synergism underscores a very valuable complementarity between jet and near room temperature studies of free radicals, whereby a simplified analysis under jet-cooled conditions can help unravel the more complicated spectra relevant to combustion diagnostics under much higher temperature conditions.

The focus of the present work is a high-resolution study of allyl radical, which after methyl³⁷ and ethyl⁴⁴ represents the third in a series of investigations

on direct absorption infrared laser spectroscopy of jet-cooled hydrocarbon radicals. Allyl is the simplest radical exhibiting resonance delocalization and one of the key radical intermediates in organic chemistry through mechanisms such as allylic halogenations, allylic substitutions, and allylic isomerizations.⁴⁵ It has been theoretically investigated since the 1950s where it was predicted to have a different sign of spin density on the terminal vs central carbon atoms.⁴⁶ Its unpaired electron occupies an (a_2) orbital, and thus allyl has a X^2A_2 ground electronic state. The allyl radical has been investigated by a variety of experimental techniques ranging from electron spin resonance^{47,48} and electron diffraction,⁴⁹ to matrix isolation,⁵⁰ REMPI,^{51,52,53} and resonance Raman⁵⁴ over the past few years. A high-resolution infrared study of the ν_{11} vibration by Hirota and co-workers⁴¹ summarizes both experimental and theoretical work up to 1992. In 1994, Hirota performed a normal coordinate analysis of the allyl radical to investigate its structure and to explain centrifugal distortion constants obtained in the ν_{11} band.⁵⁵ Ellison *et al.*⁵⁶ have studied the thermochemistry of the allyl radical, and Chen and co-workers⁵⁷ have investigated the kinetics and dynamics in photodissociation. Theoretically, isotropic hyperfine coupling constants have been calculated,⁵⁸ electronic states studied by spin-coupled valence bond theory,⁵⁹ and electron spin delocalization in the radical and ions investigated.⁶⁰ From a completely different perspective, it has been suggested that the allyl radical embedded on the surface of fullerenes might be a potential carrier of the diffuse interstellar bands.⁶¹

Aside from its fundamental value as a simple model for electronic

resonance delocalization, allyl also represents a paradigm for photochemical reaction pathways, such as unimolecular ring-closure to form cyclopropyl radical.^{50,62,63} Radical cyclization is generally of significant interest in organic chemistry since this mechanism allows the formation of a large variety of ring compounds with high regioselectivity and often very good stereoselectivity.⁴⁵ Ring strain is the most important factor in ring opening, and the formation of allyl from cyclopropyl occurs with an energy release of 23 kcal/mole.⁴⁵ Both the forward and the reverse processes have been studied theoretically⁶³ and experimentally.^{50,62} Indeed, in parallel high-resolution spectroscopic studies of cyclopropyl radical, we see direct evidence for partial ring opening of cyclopropyl radical to form allyl radical in the slit discharge environment.⁶⁴ This also indicates how high-resolution capabilities for characterization and detection of radical transients in complex mixtures can be exploited for further kinetic studies, for example, of unimolecular rearrangement dynamics.

12.2 Experiment

The allyl radical spectra are obtained with a difference frequency laser spectrometer previously described for spectroscopic studies of jet-cooled clusters.^{65,66} Allyl radicals are generated by discharging 0.5 - 0.9% allyl iodide in “Ne-70” (70% neon, 30% He), with a total backing pressure of 300-400 T behind the pulsed valve. Stainless steel electrodes spaced 300 μm apart across the length of the slit are attached to the valve body with a one mm thick insulator made of Vespel or Kel-F sandwiched between the electrodes and the valve. The valve is

grounded and a negative voltage is applied to the electrodes.^{36,37} Operating voltages are varied from -400 V to -600 V, with routinely achieved currents of about 0.5 A and current densities of ≈ 4 A/cm². These conditions yield allyl radical absorptions on the order of ≈ 0.05 - 0.10 %, which generate peak signal-to-noise ratios of ≈ 20 :1. This is in fact considerably weaker than observed for methyl³⁷ and ethyl⁴⁴ radicals where S/N ratios of 100:1-1000:1 have been achieved, but is nevertheless quite adequate for the present purposes.

A discharge-on-discharge-off data collection mode (described in Chapter 13)⁴⁴ is used to obtain the allyl radical spectral data which was useful in discriminating absorptions of unstable species from those belonging to stable molecules. In this method, the discharge is struck only during one half of the length of the gas pulse, which is normally around 1000 μ s long. The data with and without the discharge on are digitized and integrated separately and stored in two separate files. Peaks appearing both in the discharge-on and discharge-off modes can be attributed to vibrations of the radical precursor, while those in the discharge-on mode only are due to the radical. However, for the current experiments in the CH₂ antisymmetric stretch region, the spectra are essentially free of any interfering peaks. Specifically, less than 5% of the total spectral line density is present with the discharge channel turned off, i.e., can be ascribed to the allyl iodide radical precursor. This is rather different from what is observed in CH band systems of ethyl radical,⁴⁴ where some regions of strong overlap exist with the ethyl iodide spectra, and thus the discharge-on—discharge-off mode of data collection proves quite essential.

Absolute infrared frequencies are referenced to NH_3 transitions⁶⁷ observed near 3113 cm^{-1} and measured under identical slit jet expansion conditions.

Frequency stability is achieved by stabilizing the argon ion and dye lasers to ≤ 1 MHz as follows.⁶⁶ The argon ion laser is locked to a 30 cm long external Fabry-Perot cavity, which, in turn, is actively stabilized onto a fringe of a polarization-stabilized HeNe laser. Transmission fringes of the dye are scanned from the same cavity. However, for routine scanning conditions, the precision of the frequency measurement is purposely degraded by the 12 MHz scanning step size used to collect most of the allyl radical spectra. Conversely, for spin-rotation analysis of the high-resolution line profiles, the frequency step is reduced to 3 MHz, which translates into a density of at least 30-40 data points per FWHM for a single rovibrational transition.

12.3 Results and analysis

The CH_2 antisymmetric stretch region of allyl radical had been previously studied at low resolution in the matrix^{68,69} at around 3106 cm^{-1} , which greatly minimizes the difficulties of a long spectral search at high resolution. Thus, a 40 cm^{-1} region centered around 3120 cm^{-1} is scanned, yielding ≈ 200 transitions. The two CH_2 antisymmetric stretches in this region can be described as in-phase and out-of-phase, with the CH_2 subunits moving in the same direction along the C_2 axis bisecting the molecule in the in-phase stretch, and in opposite directions in the out-of-phase stretch. These two vibrations are illustrated in the upper left

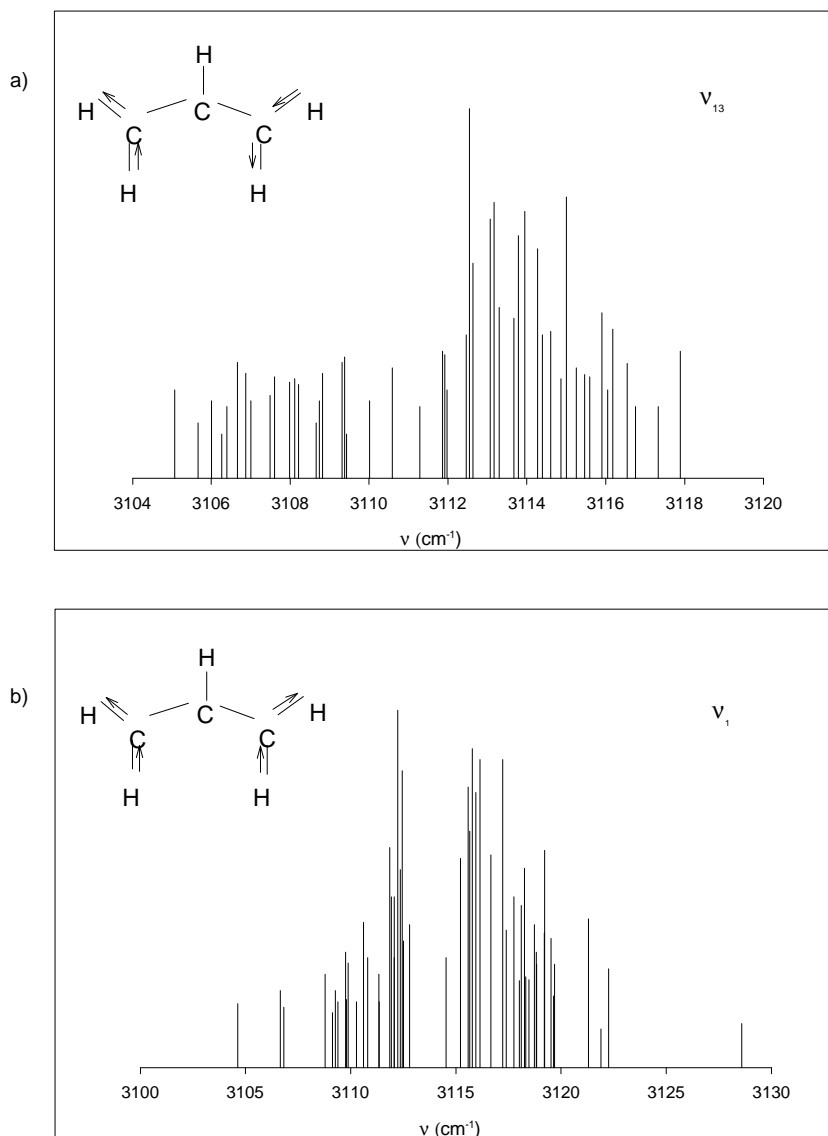


Figure 12.1 Stick plot of relative intensities for jet-cooled allyl radical in the CH₂ anti-symmetric stretch region, listing all the assigned transitions for the a) the in-phase (ν_{13}) and b) out-of-phase ν_1 bands. Intensities are taken from experiment and have been normalized with respect to the total infrared power from the difference frequency laser.

corners of Figure 12.11 (a) and (b). Since matrix studies^{68,69} suggest the in-phase stretch band (ν_1) to be considerably more intense than the out-of-phase stretch (ν_{13}) band, a search was first conducted for ν_1 .

The ν_1 in-phase vibration is a b-type band, where the change in the transition dipole moment lies along the C_2 axis. At the low rotational temperatures achieved in the slit jet discharge, the most prominent features for this band are two intense Q branches, $K_a = 1 \leftarrow 0$ and $K_a = 0 \leftarrow 1$, which are separated from each other by a gap of twice the A rotational constant. In the absence of spectral congestion, these two features are easily identified in the allyl spectra. The rest of the transitions are then readily assigned with the help of combination differences calculated from ground state constants of Hirota and co-workers.⁴¹ Fifty-two transitions are assigned, which correspond to ground state levels up to $J \leq 9$, $K_a \leq 2$. A portion of this spectrum is displayed in Figure 12.2, where the ν_1 transitions are labeled with lines above the experimental trace. The list of assigned ν_1 transitions is reported in Table 12.1(b).

The C_{2v} equilibrium structure of allyl can be unambiguously confirmed by nuclear spin statistics. Specifically, there are four hydrogen atoms in allyl that can be interchanged by a 180° rotation around the b-axis, which influences the nuclear spin statistics depending on whether $K_a + K_c$ is even or odd. For exchange of two pairs of identical spin $\frac{1}{2}$ particles, the rotational levels should have a nuclear spin weight of 10 for $(K_a + K_c) = \text{even}$, while those with $(K_a + K_c) = \text{odd}$ have a nuclear spin weight of 6. From the close up of the $Q(K_a = 0 \leftarrow 1)$ series in Figure 12.2, a 10:6 intensity alternation can be clearly observed, which further identifies allyl

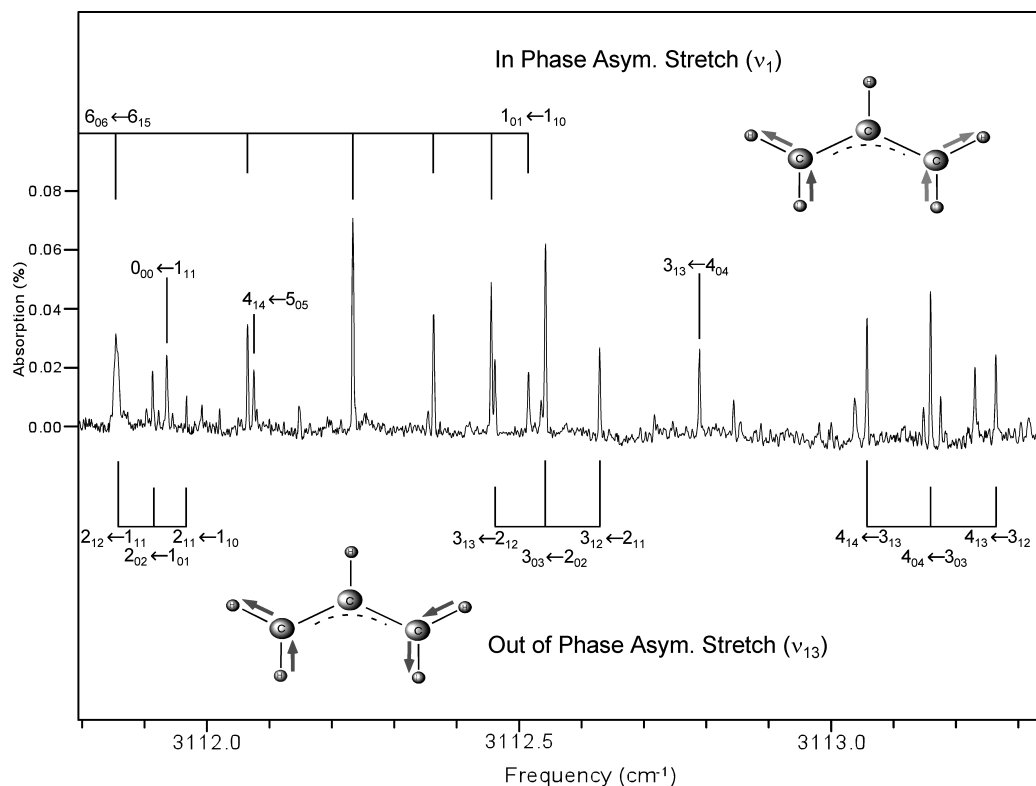


Figure 12.2 A sample data section of the allyl radical spectrum illustrating transitions in an overlapping region for both out-of-phase (ν_{13}) and in-phase (ν_1) CH_2 asymmetric stretch bands. Transitions labeled from above are for ν_1 while those labeled from below are from ν_{13} . The expected 10:6 intensity alternation due to nuclear spin statistics is clearly illustrated by the $K_a = 0 \leftarrow 1, Q(J)$ branch series in ν_1 , while the tight clusters of $\Delta K_a = 0$ transitions in the $R(J)$ branch for the ν_{13} band reflect the near prolate symmetric top behavior of allyl radical.

radical as the carrier of the IR oscillator strength.

As a first trial step in the analysis, the ν_1 spectroscopic constants are determined by least squares fitting to a standard Watson asymmetric rotor Hamiltonian (A-reduction, IR representation), while keeping the ground state constants fixed at previous determined values.⁴¹ Due to the small number of K_a levels observed, the only centrifugal distortion constants that can be meaningfully determined are Δ_{NK} and Δ_K ; with the ν_1 data all equally weighted, the standard deviation of the fit is 0.0031 cm^{-1} . Though respectably small, this is almost an order of magnitude higher than experimental uncertainty, and provides a first indication of rotational perturbations in the upper ν_1 state.

From the many strong lines remaining in the spectrum, a search is next conducted for transitions corresponding to the out-of-phase (ν_{13}) antisymmetric CH_2 stretch. Based on the structure of allyl, this band should be a-type and exhibit a structure similar to the parallel band of a near prolate symmetric top. Figure 12.2 displays several ν_{13} R branch transitions interspersed among the ν_1 lines, and denoted by standard asymmetric top notation in the lower half of the figure. Repeated clusters of $K_a = 1 \leftarrow 1$ and $K_a = 0 \leftarrow 0$ transitions for each R branch line in the ν_{13} band clearly confirm the different rotational structures anticipated for the predominantly a-type (out-of-phase) vs b-type (in-phase) antisymmetric CH_2 stretch vibration. Forty-nine additional transitions out of $K_a = 0, 1, \text{ and } 2$ are assigned for the ν_{13} band. The list of assigned ν_{13} transitions is reported in Table 12.1(a). This leaves many unassigned transitions that are most likely due to excitations out of the $K_a > 2$ sub-bands. However, since these transitions are quite

weak due to slit jet cooling, we leave these for a more detailed analysis by Curl and co-workers⁷⁰ under higher temperature conditions.

Since the preliminary analysis of the ν_1 band resulted in a fit with a standard deviation tenfold worse than experimental uncertainty, we use the combined data from both ν_1 and ν_{13} bands and the previous ν_{11} data⁴¹ to obtain an improved fit for the ground state. This is done to isolate and eliminate any effects due to spectral perturbations in the vibrationally excited manifold. A total of 36 and 17 ground state combination differences for the ν_1 and ν_{13} bands, respectively, are fitted together with 79 combination differences from Hirota *et al.*⁴¹ using a Watson's A-reduced asymmetric top Hamiltonian. Fits solely to our ground state combination difference data yield a standard deviation of 0.00046 cm^{-1} (where only a restricted set of constants A, B, C, Δ_{NK} , Δ_K , and Δ_N are utilized in the fit), which is an order of magnitude better than the initial ν_1 fit and within our reported experimental uncertainty in frequency measurement. If one includes the previous ν_{11} data,⁴¹ the standard deviation of the combined fit increases twofold to 0.00086 cm^{-1} . The two combined sets of data are weighted according to the reciprocal square of the standard deviations obtained when each set is fitted separately. The resulting parameters, including the original values reported by Hirota *et al.*,⁴¹ are listed in Table 12.2. The constants δ_K , ϕ_K , ϕ_{KN} , and ϕ_N are now determined more precisely, but with all parameters agreeing with the previous determination⁴¹ within their quoted uncertainties. However, a more extensive fit to the ground state data will be reported in the companion paper by Curl and co-workers,⁷⁰ who have taken advantage of the present jet-cooled allyl

Table 12.1 (a) Measured antisymmetric CH₂ stretch spectral transitions (obs-calc, in cm⁻¹) for the in-phase CH stretch (ν_1) band of allyl radical. (b) Measured antisymmetric CH₂ stretch spectral transitions (obs-calc, in cm⁻¹) for the out-of-phase CH stretch (ν_{13}) band of allyl radical.

N'	K_a'	K_c'	N''	K_a''	K_c''	ν	obs - calc
(a)							
7	4	3	6	3	4	3128.5376	0.0003
7	2	6	6	1	5	3122.2187	0.0015
5	2	3	4	1	4	3121.8573	-0.0115
5	2	4	4	1	3	3121.2596	0.0065
2	2	0	1	1	1	3119.6561	0.0002
2	2	1	1	1	0	3119.5987	0.0005
10	0	10	9	1	9	3119.4755	-0.0002
7	1	7	6	0	6	3119.1693	-0.0002
7	2	6	7	1	7	3119.1540	0.0017
5	2	4	5	1	5	3118.7838	0.0059
9	0	9	8	1	8	3118.7771	-0.0003
6	1	6	5	0	5	3118.6980	-0.0003
2	2	1	2	1	2	3118.4376	0.0003
2	2	0	2	1	1	3118.2706	0.0000
5	1	5	4	0	4	3118.2144	0.0002
8	0	8	7	1	7	3118.0666	0.0006
5	2	3	5	1	4	3117.9807	-0.0115
4	1	4	3	0	3	3117.7120	0.0001
7	0	7	6	1	6	3117.3451	-0.0003
3	1	3	2	0	2	3117.1862	-0.0005
6	0	6	5	1	5	3116.6204	-0.0002
6	1	5	6	0	6	3116.0990	-0.0006
5	0	5	4	1	4	3115.8975	-0.0001
4	1	3	4	0	4	3115.7400	0.0023
3	1	2	3	0	3	3115.6212	0.0039
2	1	1	2	0	2	3115.5369	0.0059
4	0	4	3	1	3	3115.1816	-0.0008
3	0	3	2	1	2	3114.4802	-0.0006
3	1	3	4	0	4	3112.7532	0.0003
1	0	1	1	1	0	3112.4710	-0.0013
2	0	2	2	1	1	3112.4112	-0.0012
3	0	3	3	1	2	3112.3186	-0.0011
4	0	4	4	1	3	3112.1901	-0.0005
4	1	4	5	0	5	3112.0308	0.0008
5	0	5	5	1	4	3112.0209	-0.0001
0	0	0	1	1	1	3111.8914	-0.0015
6	0	6	6	1	5	3111.8064	0.0005
1	0	1	2	1	2	3111.3099	-0.0014
5	1	5	6	0	6	3111.2986	0.0008
2	0	2	3	1	3	3110.7545	-0.0016
6	1	6	7	0	7	3110.5638	0.0011
3	0	3	4	1	4	3110.2241	-0.0011

Table 12.1 continued

N'	K_a'	K_c'	N''	K_a''	K_c''	v	obs - calc
7	1	7	8	0	8	3109.8305	-0.0002
4	1	3	4	2	2	3109.7602	0.0021
4	0	4	5	1	5	3109.7145	-0.0010
3	1	3	3	2	2	3109.3426	0.0005
5	0	5	6	1	6	3109.2219	-0.0006
5	1	5	5	2	4	3109.0785	-0.0005
6	0	6	7	1	7	3108.7414	0.0003
3	1	3	4	2	2	3106.7732	-0.0001
4	1	3	5	2	4	3106.6052	0.0027
2	2	0	3	3	1	3104.5798	0.0004
(b)							
12	0	12	11	0	11	3117.8483	-0.0004
11	0	11	10	0	10	3117.2796	0.0000
10	0	10	9	0	9	3116.7083	0.0013
9	1	8	8	1	7	3116.4937	-0.0003
9	0	9	8	0	8	3116.1296	0.0003
9	1	9	8	1	8	3116.0012	-0.0060
8	1	7	7	1	6	3115.8528	-0.0003
8	0	8	7	0	7	3115.5447	-0.0001
8	1	8	7	1	7	3115.4196	0.0043
7	1	6	6	1	5	3115.2067	-0.0002
7	0	7	6	0	6	3114.9520	-0.0003
7	1	7	6	1	6	3114.8224	0.0017
6	1	5	5	1	4	3114.5565	0.0002
6	0	6	5	0	5	3114.3512	0.0002
6	1	6	5	1	5	3114.2246	0.0012
5	1	4	4	1	3	3113.9021	0.0002
5	0	5	4	0	4	3113.7408	-0.0002
5	1	5	4	1	4	3113.6239	0.0004
4	1	3	3	1	2	3113.2451	0.0005
4	0	4	3	0	3	3113.1234	0.0003
4	1	4	3	1	3	3113.0213	-0.0001
3	1	2	2	1	1	3112.5851	0.0003
3	0	3	2	0	2	3112.4983	-0.0001
3	1	3	2	1	2	3112.4169	-0.0003
2	1	1	1	1	0	3111.9233	0.0002
2	0	2	1	0	1	3111.8690	0.0006
2	1	2	1	1	1	3111.8109	-0.0003
1	0	1	0	0	0	3111.2344	-0.0002
2	2	1	2	2	0	3110.5377	0.0001
0	0	0	1	0	1	3109.9609	-0.0011
1	1	1	2	1	2	3109.3772	-0.0010
1	0	1	2	0	2	3109.3264	-0.0000
1	1	0	2	1	1	3109.2657	-0.0002
2	1	2	3	1	3	3108.7691	-0.0005
2	0	2	3	0	3	3108.6940	0.0006

Table 12.1 continued

N'	K_a'	K_c'	N''	K_a''	K_c''	ν	obs - calc
2	1	1	3	1	2	3108.6010	-0.0000
3	1	3	4	1	4	3108.1605	-0.0010
3	0	3	4	0	4	3108.0648	0.0002
3	1	2	4	1	3	3107.9365	-0.0003
4	1	4	5	1	5	3107.5542	-0.0002
4	0	4	5	0	5	3107.4411	-0.0002
5	1	5	6	1	6	3106.9487	0.0002
5	0	5	6	0	6	3106.8241	-0.0005
5	1	4	6	1	5	3106.6122	0.0001
6	1	6	7	1	7	3106.3447	0.0008
6	0	6	7	0	7	3106.2152	-0.0001
6	1	5	7	1	6	3105.9531	0.0003
7	0	7	8	0	8	3105.6132	-0.0002
8	0	8	9	0	9	3105.0183	0.0000

data to assign their ν_1 band data from flash kinetic spectroscopic studies under much warmer temperature conditions.

As the next step, the two bands are least squares fit to determine the excited state parameters, with ground state constants fixed to the values determined from the combined fit. The resulting band origins and rotational constants for the ν_1 and the ν_{13} bands are reported in Table 12.3. As expected, the A, B, and C rigid asymmetric top rotational constants exhibit very little change upon vibrational excitation and are the same to within 1% in both excited and ground states. For later reference, we note that the in-phase band is $\approx 3.4 \text{ cm}^{-1}$ higher in energy than the out-of-phase vibration, despite the nominally identical “local mode” character of the CH_2 asymmetric stretch vibration on each of the terminal carbon atoms.

However, the standard deviations obtained from fits to both the ν_1 and the ν_{13} vibrations are still significantly larger than the measurement uncertainty.

Table 12.2 Ground state spectroscopic constants (in cm^{-1}) for allyl radical, obtained from least squares fits to an asymmetric top Watson Hamiltonian (A-reduction, I R representation).

	Ref. 41	this work
A	1.801890 (92)	1.801769 (52)
B	0.346320 (26)	0.346344 (10)
C	0.290219 (27)	0.2902374 (90)
$\Delta_N \times 10^7$	1.95 (73)	2.31 (49)
$\Delta_{NK} \times 10^6$	-2.15 (38)	-2.22 (35)
$\Delta_K \times 10^5$	5.23 (38)	4.65 (24)
$\delta_N \times 10^8$	4.83 (74)	4.37 (59)
$\delta_K \times 10^6$	0.86 (89)	2.16 (74)
$\phi_N \times 10^{10}$	-0.63 (60)	-0.72 (51)
$\phi_{NK} \times 10^9$	0.19 (36)	0.74 (33)
$\phi_{KN} \times 10^8$	-0.34 (36)	-0.82 (35)
$\phi_K \times 10^7$	5.03 (42)	4.48 (30)

Specifically, the least squares fitting procedure results in a standard deviation of 0.0031 cm^{-1} and 0.0012 cm^{-1} for ν_1 and ν_{13} , respectively, i.e., between threefold to tenfold worse than the fits to the ground state combination differences alone. Moreover, inspection of Tables 12.2 and 12.3 reveal that the fitted centrifugal distortion constants vary considerably between ground and excited states. These large, non-physical changes in the distortion constants and poorer fit quality provide further indication that the excited state levels are affected by perturbations. Indeed, such a difference in the ground and excited state centrifugal distortion constants had been noted previously by Hirota *et al.* in his analysis of the ν_{11} band,⁴¹ with Coriolis interactions between ν_{11} and $2\nu_7$ cited as the most probable cause.⁵⁵ We have attempted a simple two-state analysis of this interaction by including c-type Coriolis matrix elements in the rotational Hamiltonian. This however did not alter the quality of the fit, which may suggest

Table 12.3 Excited state spectroscopic constants (in cm^{-1}) for allyl radical in the in-phase (ν_1) and out-of-phase (ν_{13}) antisymmetric CH_2 stretch vibrations. These results are obtained from least squares fits to an asymmetric top Watson Hamiltonian (A-reduction, I R representation).

	ν_1	ν_{13}
A	1.78158 (45)	1.80257 (51)
B	0.345569 (83)	0.345998 (15)
C	0.289917 (39)	0.2899978 (84)
$\Delta_{\text{NK}} \times 10^6$	-116 (15)	-
$\Delta_{\text{K}} \times 10^5$	19.7 (47)	391 (15)
ν_0	3113.98488 (89)	3110.59857 (36)

that more than two states are involved. A detailed analysis of this perturbation structure will be available from the flash kinetic spectroscopic studies obtained at higher temperatures, which therefore sample a more extensive range of thermally populated J, K_a manifolds.⁷⁰

As a final note in this section, it is interesting to compare the relative intensities of the two ν_1 and ν_{13} bands. The distribution of rotational levels in the allyl radical is close to thermal; Figs. 12.3 (a) and (b) show standard Boltzmann plots of the spectral data, which can be reasonably well fitted with a temperature of 18 ± 2 K for the ν_1 band and 21 ± 2 K for the ν_{13} band. From these plots, the relative band strengths can be estimated by summing up all transition intensities from an equivalent asymmetric top spectrum calculated at an average temperature of 20 K. This procedure yields an integrated band strength for ν_{13} that is weaker

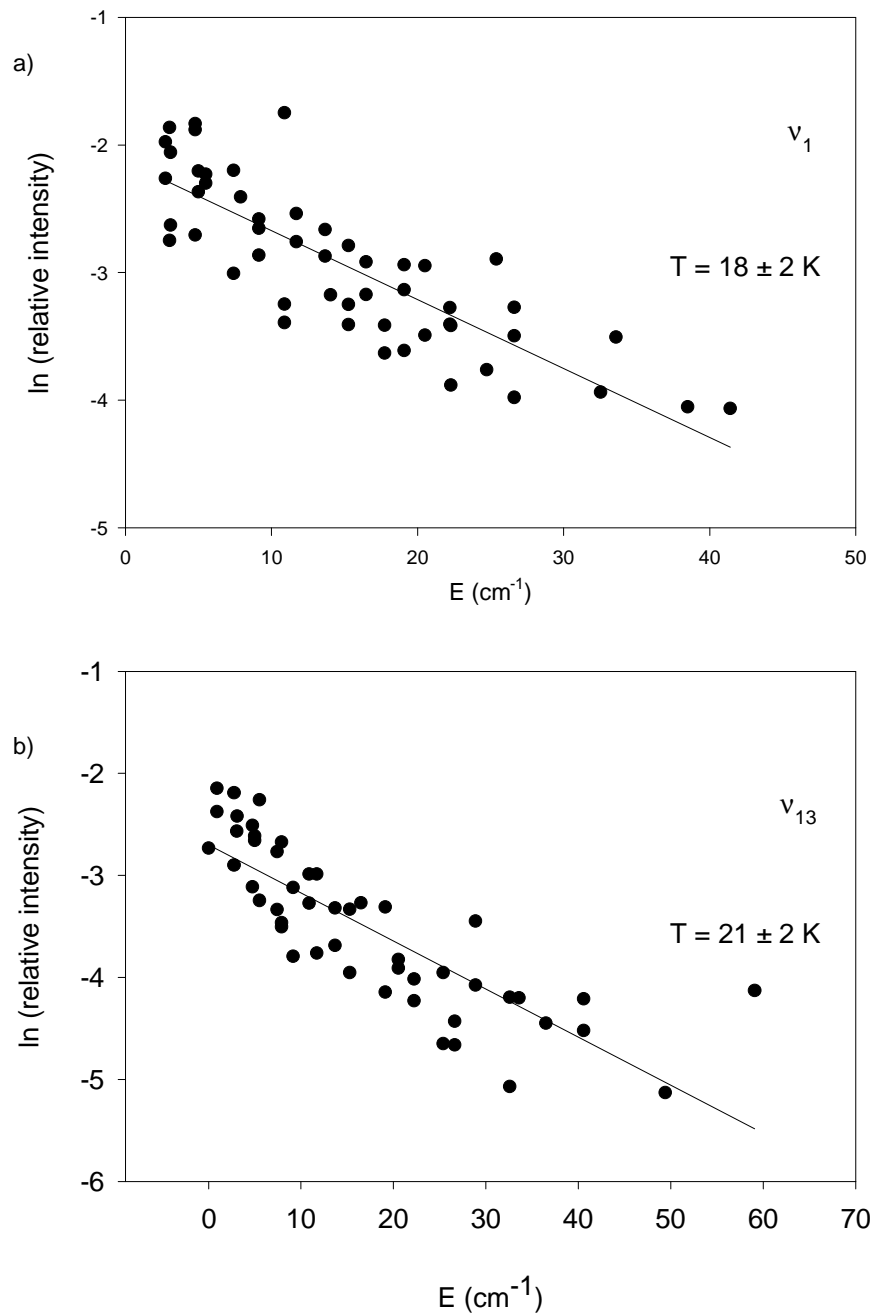


Figure 12.3 Boltzmann plots for experimentally observed intensities in the ν_1 (a) and ν_{13} (b) bands, showing the near thermal distribution of jet cooled rotational levels with temperatures on the order of $\approx 20\text{K}$.

than ν_1 by approximately 1.5. This is considerably different from *ab initio* calculations,⁷² which predict a much larger ratio of ≈ 7 -8:1. These results can be interpreted qualitatively in the context of a simple bond dipole model for the two CH_2 local mode vibrations, where one computes the vector sum/difference for two transition dipoles corresponding, respectively, to in-phase/out-of-phase CH_2 antisymmetric excitation. For a local mode antisymmetric stretch transition dipole perpendicular to the CH_2 bisector, this model correctly predicts a stronger in-phase vs. out-of-phase vibration intensity, though only in the intensity ratio 3:1. This is threefold smaller than predicted from *ab initio* calculations,⁷² but much closer to the 1.5:1 ratio observed experimentally.

12.4 Discussion

In the analysis of the CH_2 stretches, excess broadening beyond the normal residual Doppler contribution is observed in many of the allyl radical lines. Specifically, from our experience with species of comparable mass in a He:Ne expansion mix, the jet-cooled discharge expansion typically yields sub-Doppler line widths of ≈ 60 -70 MHz. Indeed, many of the lines in the out-of-phase (ν_{13}) a-type band exhibit widths as narrow as this prediction. However, low J lines in the in-phase (ν_1) b-type band are broadened by as much as ~ 120 MHz, in particular for $\Delta K_a = 1$ transitions into the higher K_a states. This is qualitatively similar to what was reported by Hirota *et al.*, who observed high K_a transitions in the ν_{11} band with excess line widths and attributed this effect to unresolved splitting from spin-rotation interaction.⁴¹ However, due to room temperature Doppler

broadening and diode laser frequency noise, a more detailed analysis was not pursued in the earlier studies. Since the current jet-cooled measurements are obtained under higher resolution sub-Doppler conditions, the data offer an opportunity to extract an improved estimate of these spin rotation effects.

The allyl radical possesses electronic angular momentum due to its unpaired electron. The orbital angular momentum of the electron is largely quenched, but its spin (\mathbf{S}) can couple to the overall molecular rotation (\mathbf{N}) to form the total angular momentum $\mathbf{J} = \mathbf{N} + \mathbf{S}$. Neglecting centrifugal distortion contributions, the spin-rotation interaction Hamiltonian is given by

$$H_{\text{spin rotation}} = 1/2 (\epsilon_{aa} N_a S_a + \epsilon_{bb} N_b S_b + \epsilon_{cc} N_c S_c) \quad (12.1)$$

where the spin-rotation interaction constants ϵ_{aa} , ϵ_{bb} , and ϵ_{cc} scale roughly with the spin-orbit coupling constant and the A, B, and C rotational constants, respectively. In our previous studies of the methyl radical,³⁷ such spin rotation structure is fully resolved with the sub-Doppler resolution capabilities of the slit-jet spectrometer. For the allyl radical spectra, however, the fine structure effects are much smaller and not fully resolved, which justifies a more limited scope of analysis. For example, as indicated by Hirota *et al.*,⁴¹ the largest spin rotation effect is expected to arise from a-axis rotation (ϵ_{aa}) with smaller contributions from tumbling around the b and c axes (ϵ_{bb} and ϵ_{cc}). This is confirmed by the experimental line widths, which are quite noticeably broadened for b-type $K_a = 2 \leftarrow 1$ and $1 \leftarrow 0$ transitions (i.e., most sensitive to ϵ_{aa}), with near instrument limited line widths for the a-type $K_a=0 \leftarrow 0$ and $1 \leftarrow 1$ transitions (i.e., most sensitive to ϵ_{bb} and ϵ_{cc}). Thus, we first limit the analysis to only the a-axis contributions to spin rotation, and then

investigate the influence of relaxing this constraint.

To extract the spin rotation information, a series of transitions in the ν_1 ($K_a = 2 \leftarrow 1, 1 \leftarrow 0$) and ν_{13} ($K_a = 1 \leftarrow 1$ and $0 \leftarrow 0$) bands are scanned multiple times under high-resolution conditions (i.e., 2 - 4 MHz step size). The transitions are then included in a least-squares fit to the data as follows. The eigenvalues and eigenvectors for a given J are obtained by explicit diagonalization in a symmetric top basis of

$$H = H_{\text{rotor}} + H_{\text{spin rotation}} \quad (12.2)$$

where H_{rotor} is the rigid asymmetric rotor Hamiltonian and $H_{\text{spin rotation}}$ is given by Eq (12.1). The spectra are predicted by energy differences, with relative intensities for each spin-rotation transition obtained from the eigenvectors by standard Clebsch-Gordon algebra.⁷¹ The net transition line shape is then determined by convolving the individual spin-rotation components over a common Gaussian profile representing the instrumental sub-Doppler limit ($\Delta v_{\text{Doppler}}$). Two parameters are floated in the fit: i) ϵ_{aa} , which is taken to be the same in the ground and excited states, and ii) the Gaussian line width of an individual spin-rotation component. These are then optimized in a least squares sense to fit the high-resolution line profiles, yielding $\epsilon_{aa} \approx -48$ MHz and $\Delta v_{\text{Doppler}} \approx 75$ MHz. As a further test of these results, we next relax the constraint on ϵ_{bb} and ϵ_{cc} in the least squares fits and allow all three spin rotation parameters to float. The converged results indicate a somewhat larger negative value of $\epsilon_{aa} \approx -67$ MHz, but with strong correlation between ϵ_{bb} and ϵ_{cc} . This represents our best estimate of ϵ_{aa} ; however, the sensitivity to inclusion of ϵ_{bb} and ϵ_{cc} suggests an uncertainty as large

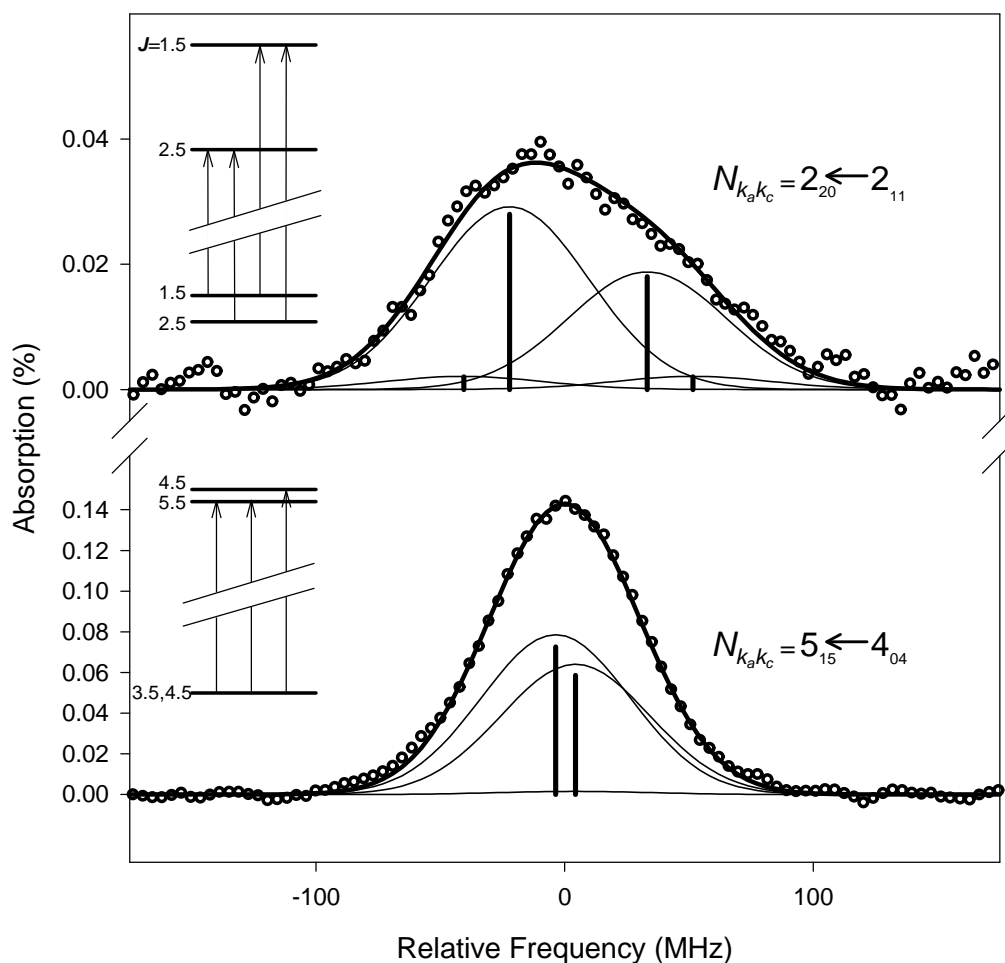


Figure 12.4 Sample data indicating quantum state excess broadening due to spin-rotation interactions in allyl radical. Each transition reflects the sum of multiple overlapping Gaussians from individual spin-rotation components, where the relative intensities and frequencies are determined from matrix diagonalization of a combined rigid asymmetric top and spin rotation Hamiltonian (see text for details). Note the substantially larger broadening in the $2_{20} \leftarrow 2_{11}$ transition vs. the $5_{15} \leftarrow 4_{04}$ transition. This reflects the greater splittings observed in higher K_a states as well as for states with $J \approx K_a$, due to the predominance of spin-rotation effects for rotation around the a-axis.

as ± 25 MHz. This value is smaller than but not inconsistent with the previous analysis of Hirota *et al.*⁴¹ for the ν_{11} band, who estimated the magnitude of $|\epsilon_{aa}| \approx 100$ MHz, with 200 MHz as a conservative upper limit by ascribing the line widths entirely to a-axis spin-rotation broadening. It is worth noting that the sign of ϵ_{aa} could not be determined in the work of Hirota *et al.*,⁴¹ since intensities of the two dominant fine structure transitions are equal in the high N limit. Indeed, the sign is most sensitive to *asymmetry* in the line shapes, which is only evident for the low rotational states accessed under supersonic expansion conditions. A sample data scan and corresponding line profile analysis is shown in Figure 12.4, which indicates quite good agreement between experimental data and the least squares predictions.

In a purely local mode picture for the CH_2 antisymmetric stretch vibrations, there would be no coupling between “right” and “left” CH_2 groups, and thus the two in-phase and out-of-phase bands would be exactly degenerate. This is of course nearly true, with a 3.4 cm^{-1} splitting of only $\approx 1/1000$ of the vibrational frequencies. On the other hand, this makes it interesting to speculate on possible sources of the splitting between the two bands, and in particular suggests the use of simple perturbation theory to estimate the magnitude of these effects. For localized vibrations in close proximity, kinetic coupling can be quite significant; for example, this is a major source of the splitting between symmetric and asymmetric CH stretches in the same CH_2 subunit. However, this effect would be expected to drop off rapidly with the number of intervening atoms, particularly for moderately heavy atoms such as in the C-C-C frame. Furthermore,

this kinetic coupling should be especially small in allyl radical, since motion in the antisymmetric stretch coordinate nominally produces no component of momentum transfer parallel to the adjacent C-C bond. A similar argument would apply to potential coupling, which would also be expected to drop off rapidly with distance.

On the other hand, a form of potential coupling that can be significant is the long-range electrostatic coupling between the two CH₂ subunits, which may be approximated in lowest order by two dipoles separated by a distance r . This interaction is given by

$$V_{ab} = \frac{\mu_a \mu_b}{r_{ab}^3} [-2 \cos \theta_a \theta_b + \sin \theta_a \sin \theta_b \cos (\phi_b - \phi_a)] \quad (12.3)$$

where μ_a and μ_b refer to the dipole moments of the two CH₂ subunits, and θ and ϕ characterize the orientation of the dipoles with respect to r_{ab} . From second order degenerate perturbation theory, the splitting between the two bands quantum mechanically reflects the off diagonal matrix element of Eq. (12.3) between the two degenerate “local mode” antisymmetric stretch excitations on each of the CH₂ subunits, i.e., $\langle 0, 1 | V_{ab} | 1, 0 \rangle$. By expansion of the μ_a and μ_b dipole operators in a Taylor series, and re-expressing the displacements in terms of raising/lowering operators, this matrix element can be shown to be

$$\langle 0, 1 | V_{ab} | 1, 0 \rangle = |\langle 1 | \mu_a | 0 \rangle|^2 / r_{ab}^3 [-2 \cos \theta_a \cos \theta_b + \sin \theta_a \sin \theta_b \cos (\phi_b - \phi_a)] \quad (12.4)$$

where $|\langle 1 | \mu_a | 0 \rangle|$ is the local mode dipole transition moment for each CH₂ local

mode vibration. The integrated transition strength for the local mode CH₂ stretch can be estimated to be approximately one-half of the combined *ab initio* intensities calculated for the in-phase/out-of-phase vibrations,⁷² which yields $S_0 \approx 3.70 \times 10^{-18}$ cm/molecule and $|\langle 1|\mu_a|0\rangle| \approx 0.054$ D. The distance and angles between transition dipoles centered on the two outer C atoms can be estimated from the *ab initio* structural parameters for allyl radical.⁷² When inserted in Eq. (5), this yields a dipole-dipole induced splitting of $\approx +2.1$ cm⁻¹, i.e., more than half of the experimentally observed value of +3.4 cm⁻¹. This estimate is not intended to suggest that electrostatic coupling is the only contribution; however, it does predict the correct sign and approximate magnitude of the in-phase vs. out-of-phase vibrational splitting.

As a final note, these high-resolution direct absorption methods also permit the absolute density of the allyl radicals in slit jet discharge to be extracted. From the thermal Boltzmann plots in Figure 12.3, the integrated absorbances for the ν_1 and ν_{13} bands can be estimated to be $S_0 \approx 1.2 \times 10^{-4}$ cm⁻¹ and 7.8×10^{-5} cm⁻¹, respectively. The combined strength is $\approx 2.0 \times 10^{-4}$ cm⁻¹, which when scaled by *ab initio* integrated absorption strengths for both bands of $\approx 7.4 \times 10^{-18}$ cm/radical,⁷² yields a column integrated density of allyl radicals of $\approx 2.7 \times 10^{13}$ radicals/cm². For an 80 cm path length multipass through the expansion, this translates into a total number density of $\approx 3.4 \times 10^{11}$ jet-cooled allyl radicals/cm³ in the IR laser probe region 1 cm downstream from the slit. Based on a 1/r concentration drop off for a 1D expansion and a 300 μ m slit width, this implies an

allyl density of $\approx 1.0 \times 10^{13}$ radicals/cm³ at the discharge nozzle orifice. These estimates indicate substantially less efficient generation of allyl radical in the discharge than previously observed in the smaller hydrocarbon species such as methyl radical,³⁷ where densities $\geq 10^{14}$ radicals/cm³ have been observed for comparable partial pressures of radical precursor, expansion conditions, etc. Nevertheless, these nozzle densities are still remarkably high and already adequate for high-resolution spectroscopy of even larger hydrocarbon radicals via high sensitivity direct absorption methods.

12.5 Summary

The combination of high sensitivity direct absorption methods and long path length, slit discharge, supersonic expansions have been used to obtain high-resolution IR spectra of jet-cooled allyl radical under low temperature ($T_{\text{rot}} \approx 20\text{K}$) conditions. The two bands observed correspond to in-phase and out-of-phase combinations of the two local mode antisymmetric CH₂ stretch vibrations on each end of the molecule. The high-resolution data have been successfully analyzed with a Watson asymmetric rotor Hamiltonian, yielding precise band origins and rotational constants for both bands. The high quality of least squares fits to ground state combination differences indicate that the rotational level structure in the lower state is well behaved. The reduced quality of fits to the vibrational transitions, on the other hand, suggest the presence of Coriolis mediated rotational perturbations in the upper state. However, this is a topic much better suited to the larger range of J, K_a quantum state data obtained from higher temperature studies,

as will be explicitly discussed elsewhere by Curl and co-workers.⁷⁰ In combination with other work on methyl³⁶ and ethyl radicals,⁴⁴ the current study of allyl radical underscores the wide range of open shell hydrocarbon radical systems that will become experimentally accessible via slit discharge methods at both high spectral resolution and low rotational temperatures.

References for Chapter 12

- ¹ S. S. Lee, D. W. Minsek, D. J. Vestyck, and P. Chen, *Science* **263**, 1596 (1994).
- ² G. A. Olah and Á. Molnár, *Hydrocarbon Chemistry* (John Wiley & Sons, Inc., New York, 1995).
- ³ E. Herbst, *Ann. Rev. Phys. Chem.* **46**, 27 (1995).
- ⁴ M. M. Maricq, J. J. Szente, G. A. Khitrov, and J. S. Francisco, *J. Phys. Chem.* **100**, 4514 (1995).
- ⁵ T. Suzuki and E. Hirota, *J. Chem. Phys.* **98**, 2387 (1993).
- ⁶ J. D. Adamson, C. L. Morter, J. D. DeSain, G. P. Glass, and R. F. Curl, *J. Phys. Chem.* **100**, 2125 (1996).
- ⁷ E. Hirota and K. Kawaguchi, *Ann. Rev. Phys. Chem.* **46**, 53 (1985).
- ⁸ L. Hall, D. Zeitz, J. W. Stephens, J. V. V. Kasper, G. P. Glass, R. F. Curl, and F. K. Tittel, *J. Phys. Chem.* **90**, 2501 (1986).
- ⁹ P. A. Tesner, *Combust. Explos. Shock Waves* **28**, 254 (1992).
- ¹⁰ J. A. Miller, R. J. Kee, and C. K. Westbrook, *Ann. Rev. Phys. Chem.* **41**, 345 (1990).
- ¹¹ G. A. Laguna and S. L. Baughcum, *Chem. Phys. Lett.* **88**, 568 (1982).
- ¹² P. B. Davies and P. M. Martineau, *Appl. Phys. Lett.* **57**, 237 (1990).
- ¹³ S. K. Loh and J. M. Jasinski, *J. Chem. Phys.* **95**, 4914 (1991).
- ¹⁴ K. C. Herr and G. C. Pimentel, *Appl. Optics*, **4**, 25 (1965).
- ¹⁵ L. Y. Tan, A. M. Winer, and G. C. Pimentel, *J. Chem. Phys.* **57**, 4028 (1972).
- ¹⁶ R. F. Curl, K. K. Murray, M. Petri, M. L. Richnow, and F. K. Tittel, *Chem. Phys. Lett.* **161**, 98 (1989).
- ¹⁷ H. Petek, D. J. Nesbitt, P. R. Ogilby, and C. B. Moore, *J. Phys. Chem.* **87**, 5367

(1983).

- ¹⁸ T. J. Sears, W. M. Fawzy, and P. M. Johnson, *J. Chem. Phys.* **97**, 3996 (1992).
- ¹⁹ A. McIlroy and F. P. Tully, *J. Chem. Phys.* **99**, 3597 (1993).
- ²⁰ J. F. Hershberger, S. A. Hewitt, G. W. Flynn, and R. E. Weston, Jr., *J. Chem. Phys.* **88**, 7248 (1988).
- ²¹ A. Schiffman, D. D. Nelson, Jr., M. S. Robinson, and D. J. Nesbitt, *J. Phys. Chem.* **95**, 2629 (1991).
- ²² C. A. Taatjes, *J. Chem. Phys.* **106**, 1786 (1997).
- ²³ R. E. Smalley, B. L. Ramakrishna, D. H. Levy, and L. Wharton, *J. Chem. Phys.* **61**, 4363 (1974).
- ²⁴ R. E. Smalley, L. Wharton, and D. H. Levy, *J. Chem. Phys.* **63**, 4977 (1975).
- ²⁵ T. G. Dietz, M. A. Duncan, D. E. Powers, and R. E. Smalley, *J. Chem. Phys.* **74**, 6511 (1981).
- ²⁶ see for instance D. W. Kohn, H. Clauberg, and P. Chen, *Rev. Sci. Inst.* **63**, 4003 (1992).
- ²⁷ A. T. Droege and P. C. Engelking, *Chem. Phys. Lett.* **96**, 316 (1983).
- ²⁸ X. Q. Tan, T. G. Wright, and T. A. Miller in *Jet Spectroscopy and Molecular Dynamics*, edited by J. M. Hollas and D. Phillips (Blackie Academic and Professional, London, 1995).
- ²⁹ A. Van Orden, R. A. Provencal, F. N. Keutsch, and R. J. Saykally, *J. Chem. Phys.* **105**, 6111 (1996).
- ³⁰ M. Ishiguro, T. Imajo, K. Harada, M. Matsubara, K. Tanaka, and T. Tanaka, *Chem. Phys. Lett.* **263**, 629 (1996).
- ³¹ G. Hilpert, H. Linnartz, M. Havenith, J. J. ter Meulen, and W. L. Meerts, *Chem. Phys. Lett.* **219**, 384 (1994).
- ³² Y. Xu, M. Fukushima, T. Amano, and A. R. W. McKellar, *Chem. Phys. Lett.* **242**, 126 (1995).

- ³³ K. C. Comer and S. C. Foster, *Chem. Phys. Lett.* **202**, 216 (1993).
- ³⁴ M. C. McCarthy, M. J. Travers, A. Kovacs, C. A. Gottlieb, and P. Thaddeus, *Astrophys. J. Supplement Series* **113**, 105 (1997).
- ³⁵ M. C. McCarthy, M. J. Travers, C. A. Gottlieb, and P. Thaddeus, *Astrophys. J. Lett.* **483**, L139 (1997).
- ³⁶ D. T. Anderson, S. Davis, T. S. Zwier, and D. J. Nesbitt, *Chem. Phys. Lett.* **258**, 207 (1996).
- ³⁷ S. Davis, D. T. Anderson, G. Duxbury, and D. J. Nesbitt, *J. Chem. Phys.* **107**, 5661 (1997).
- ³⁸ K. Hoshina, H. Kohguchi, A. Y. Oshima, and Y. Endo, *J. Chem. Phys.* **108**, 3465 (1998).
- ³⁹ P. G. Carrick, A. J. Merer, and R. F. Curl, Jr. *J. Chem. Phys.* **78**, 3652 (1983).
- ⁴⁰ C. L. Morter, C. Domingo, S. K. Farhat, E. Cartwright, G. P. Glass, and R. F. Curl, *Chem. Phys. Lett.* **195**, 316 (1992).
- ⁴¹ E. Hirota, C. Yamada, and M. Okunishi, *J. Chem. Phys.* **97**, 2963 (1992).
- ⁴² T. J. Sears, J. M. Frye, V. Spirko, and W. P. Kramer, *J. Chem. Phys.* **90**, 2125 (1989).
- ⁴³ T. J. Sears, P. M. Johnson, P. Jin, and S. Oatis, *J. Chem. Phys.* **104**, 781 (1996).
- ⁴⁴ S. Davis, D. Uy, and D. J. Nesbitt (manuscript in preparation).
- ⁴⁵ J. Fossey, D. Lefort, and J. Sorba, *Free Radicals in Organic Chemistry* (John Wiley & Sons, Chichester, 1995).
- ⁴⁶ C. Heller and T. Cole, *J. Chem. Phys.* **37**, 243 (1962) and references therein.
- ⁴⁷ R. W. Fessenden and R. H. Schuler, *J. Chem. Phys.* **39**, 2147 (1963).
- ⁴⁸ H. J. McManus, R. W. Fessenden, and D. M. Chipman, *J. Phys. Chem.* **92**, 3778 (1988).
- ⁴⁹ E. Vajda, J. Tremmel, B. Rozsondai, I. Hargittai, A. K. Mal'tsev, N. Kagramanov, and O. M. Nefedov, *J. Am. Chem. Soc.* **108**, 4352 (1986).

- ⁵⁰ K. Holtzhauer, C. Cometta-Morini, and J. F. M. Oth, *J. Phys. Org. Chem.* **3**, 219 (1990).
- ⁵¹ D. W. Minsek and P. Chen, *J. Phys. Chem.* **97**, 13375 (1993).
- ⁵² D. W. Minsek, J. A. Blush, and P. Chen, *J. Phys. Chem.* **96**, 2025 (1992).
- ⁵³ J. A. Blush, D. W. Minsek, and P. Chen, *J. Phys. Chem.* **96**, 10150 (1992).
- ⁵⁴ X. Liu, J. D. Getty, and P. B. Kelly, *J. Chem. Phys.* **99**, 1522 (1993).
- ⁵⁵ E. Hirota, *J. Mol. Struct.* **320**, 75 (1994).
- ⁵⁶ G. B. Ellison, G. E. Davico, V. M. Bierbaum, and C. H. DePuy, *Int. J. Mass Spectrom. Ion Processes* **156**, 109 (1996).
- ⁵⁷ H. J. Deyerl, T. Gilbert, I. Fischer, and P. Chen, *J. Chem. Phys.* **107**, 3329 (1997).
- ⁵⁸ S. A. Perera, L. M. Salemi, and R. J. Bartlett, *J. Chem. Phys.* **106**, 4061 (1997).
- ⁵⁹ J. M. Oliva, J. Gerratt, D. L. Cooper, P. B. Karadakov, and M. Raimondi, *Chem. Phys.* **106**, 3663 (1997).
- ⁶⁰ Y. Mo, Z. Lin, W. Wu, and Q. Zhang, *J. Phys. Chem.* **100**, 6469 (1996).
- ⁶¹ A. Webster, *Mon. Not. R. Astron. Soc.* **265**, 421 (1993).
- ⁶² J. D. Getty, M. J. Burmeister, S. G. Westre, and P. B. Kelly, *J. Am. Chem. Soc.* **113**, 801 (1991).
- ⁶³ S. Olivella, A. Solé, and J. M. Bofill, *J. Am. Chem. Soc.* **112**, 2160 (1990).
- ⁶⁴ S. Davis, D. Uy, S. Kable and D. J. Nesbitt (work in progress).
- ⁶⁵ C. M. Lovejoy and D. J. Nesbitt, *J. Chem. Phys.* **86**, 3151 (1987).
- ⁶⁶ E. Riedle, S. H. Ashworth, J. T. Farrell, Jr., and D. J. Nesbitt, *Rev. Sci. Instrum.* **65**, 42 (1994).
- ⁶⁷ G. Guelachvilli and K. N. Rao, *Handbook of Infrared Standards II* (Academic Press, Inc. Boston, 1993).

- ⁶⁸ G. Maier, H. P. Reisenauer, B. Rohde, and K. Dehnicke, *Chem. Ber.* **116**, 732 (1983).
- ⁶⁹ A. K. Mal'tsev, V. A. Korolov, and O. M. Nefedov, *Bull. Acad. Sci. USSR, Div. Chem. Sci.* **31**, 2131 (1982).
- ⁷⁰ J. D. DeSain, R. I. Thompson, S. D. Sharma, and R. F. Curl, *J. Chem. Phys.* (submitted).
- ⁷¹ C. H. Townes, and A. L. Schawlow, *Microwave Spectroscopy* (New York, McGraw-Hill, 1955).
- ⁷² P. G. Szalay, A. G. Császár, and G. Fogarasi, *J. Chem. Phys.* **93**, 1246 (1990).

